Inorg. Chem. **2009**, *48*, 3360−3370

Forum

Functional Coordination Nanoparticles

Laure Catala, Florence Volatron, Daniela Brinzei, and Talal Mallah*

Institut de Chimie Moléculaire et des Matériaux d'Orsay (ICMMO), CNRS, Université Paris-Sud 11, 91405 Orsay, France

Received July 5, 2008

Designing new objects in the perspective of creating useful functionalities at the nanoscale has been the subject of intense research efforts during the last 20 years. Coordination nanoparticles (CNPs) emerged less than 10 years ago, opening new possibilities for the design of bistable molecule-based objects where magnetism may be controlled or tuned by an external perturbation (light irradiation, temperature change, magnetic field, etc.). Magnetic cyanide-bridged networks have been shown to possess the potential to be shaped as nanoparticles, leading to new functionalities. Light- and temperature-induced bistable nanoparticles were thus discovered. Luminescent CNPs were also prepared, demonstrating the large potential of these objects.

Introduction

The study of extended networks containing magnetic metal ions has been the subject of intense research efforts during the last 20 years. Room temperature magnets based on coordination networks (or metal−organic frameworks, which are the same) have been reported in 1991 and 1995.[1,2] The design of networks where magnetism coexists with another property (optical, conducting, chiral, porosity, etc.) and in some cases where the bulk magnetic behavior can be controlled by external stimuli (light, temperature, and pressure) was also achieved, opening the perspectives for useful functionalities.[3−36] In parallel, many research efforts have been devoted during the past few years to the design of nanostructures of these magnetic materials in order to investigate the size reduction effects on their functionality and potential applications, with the perspective of integrating them into devices.[37−77] In this paper, we report our recent results on the preparation and properties of nanostructured magnetic coordination networks called coordination nano-

* To whom correspondence should be addressed. E-mail: mallah@icmo.u-psud.fr. Tel: (+33) (0)1 69 15 47 49. Fax: (+33) (0)1 69 15 47 54.

(1) Manriquez, J. M.; Yee, G. T.; Mclean, R. S.; Epstein, A. J.; Miller, J. S. *Science* **1991**, *252*, 1415–1417.
(2) Ferlay, S.; Mallah, T.; Ouahes, R.; Veillet, P.; Verdaguer, M. *Nature* **1995**, *378*, 701–703.
(3) Sato, O.; Iyoda, T.; Fujishima, A.; Hashimoto, K. *Science* **1996**, *272*, 704–705.
(4) Kahn, O.; Martinez, C. J. *Science* **1998**, *279*, 44–48.
(5) Andres, R.; Gruselle, M.; Malezieux, B.; Verdaguer, M.; Vaissermann, J. *Inorg. Chem.* **1999**, *38*, 4637–4646.
(6) Decurtins, S.; Pellaux, R.; Antorrena, G.; Palacio, F. *Coord. Chem. Rev.* **1999**, *192*, 841–854.
(7) Bleuzen, A.; Lomenech, C.; Escax, V.; Villain, F.; Varret, F.; Moulin, C. C. D.; Verdaguer, M. *J. Am. Chem. Soc.* **2000**, *122*, 6648–6652.
(8) Coronado, E.; Clemente-Leon, M.; Galan-Mascaros, J. R.; Gimenez-Saiz, C.; Gomez-Garcia, C. J.; Martinez-Ferrero, E. *J. Chem. Soc., Dalton Trans.* **2000**, 3955–3961.
(9) Coronado, E.; Galan-Mascaros, J. R.; Gomez-Garcia, C. J.; Laukhin, V. *Nature* **2000**, *408*, 447–449.
(10) Coronado, E.; Galan-Mascaros, J. R.; Gomez-Garcia, C. J.; Martinez-Agudo, J. M. *Synth. Met.* **2001**, *122*, 501–507.
(11) Evans, J. S. O.; Benard, S.; Yu, P.; Clement, R. *Chem. Mater.* **2001**, *13*, 3813–3816.
(12) Niel, V.; Martinez-Agudo, J. M.; Munoz, M. C.; Gaspar, A. B.; Real, J. A. *Inorg. Chem.* **2001**, *40*, 3838–3839.
(13) Ohkoshi, S.; Machida, N.; Zhong, Z. J.; Hashimoto, K. *Synth. Met.* **2001**, *122*, 523–527.
(14) Rombaut, G.; Verelst, M.; Golhen, S.; Ouahab, L.; Mathoniere, C.; Kahn, O. *Inorg. Chem.* **2001**, *40*, 1151–1159.
(15) Halder, G. J.; Kepert, C. J.; Moubaraki, B.; Murray, K. S.; Cashion, J. D. *Science* **2002**, *298*, 1762–1765.
(16) Alberola, A.; Coronado, E.; Galan-Mascaros, J. R.; Gimenez-Saiz, C.; Gomez-Garcia, C. J. *J. Am. Chem. Soc.* **2003**, *125*, 10774–10775.
(17) Maspoch, D.; Ruiz-Molina, D.; Wurst, K.; Domingo, N.; Cavallini, M.; Biscarini, F.; Tejada, J.; Rovira, C.; Veciana, J. *Nat. Mater.* **2003**, *2*, 190–195.
(18) Sato, Y.; Ohkoshi, S.; Arai, K.; Tozawa, M.; Hashimoto, K. *J. Am. Chem. Soc.* **2003**, *125*, 14590–14595.
(19) Tokoro, H.; Ohkoshi, S.; Hashimoto, K. *Appl. Phys. Lett.* **2003**, *82*, 1245–1247.
(20) Coronado, E.; Day, P. *Chem. Rev.* **2004**, *104*, 5419–5448.
(21) Kitagawa, S.; Kitaura, R.; Noro, S. *Angew. Chem., Int. Ed.* **2004**, *43*, 2334–2375.
(22) Maspoch, D.; Ruiz-Molina, D.; Veciana, J. *J. Mater. Chem.* **2004**, *14*, 2713–2723.

10.1021/ic8012574 CCC: $40.75
Published on Web 04/13/2009

particles (CNPs) that are mainly based on bimetallic cyanide-bridged systems. Also, in order to show the generality of the approach and the potentiality of coordination networks to be structured at the nanoscale, we describe the synthesis and luminescent behavior of terephthalate-bridged lanthanide nanoparticles that may find applications as biological labels and/or contrast agents.[74,78]

CNPs are a class of materials that combine the flexibility of the electronic structure and the versatile architecture of coordination systems (0-, 1-, 2-, and 3D) providing new functionalities at the nanoscale. CNPs are obtained using a bottom-up approach; they may be divided into three types depending on the dimensionality of the coordination bonds throughout the particle.

Type I: CNPs are prepared from the reaction of a transition-metal complex (ML_6) and a bridging ligand (BL) through a substitution reaction, leading to coordination bonds in the three directions of space.[42,43,47,53,55,59,62,68,76,78] The only reaction taking place for the formation of such particles is the substitution of a ligand in the coordination sphere of the ML_6 building block by the BL, while for other particles (oxides, sulfides, metallic, etc.), other reactions may occur. Thus, the substitution reaction plays a central role in the formation of type I CNP and the control of their size and dispersity. A deep knowledge of the mechanism of the

(23) Ohkoshi, S. I.; Arai, K. I.; Sato, Y.; Hashimoto, K. *Nat. Mater.* **2004**, *3*, 857–861.
(24) Pointillart, F.; Train, C.; Gruselle, M.; Villain, F.; Schmalle, H. W.; Talbot, D.; Gredin, P.; Decurtins, S.; Verdaguer, M. *Chem. Mater.* **2004**, *16*, 832–841.
(25) Bonhommeau, S.; Molnar, G.; Galet, A.; Zwick, A.; Real, J. A.; McGarvey, J. J.; Bousseksou, A. *Angew. Chem., Int. Ed.* **2005**, *44*, 4069–4073.
(26) Coronado, E.; Gimenez-Lopez, M. C.; Levchenko, G.; Romero, F. M.; Garcia-Baonza, V.; Milner, A.; Paz-Pasternak, M. *J. Am. Chem. Soc.* **2005**, *127*, 4580–4581.
(27) Galet, A.; Gaspar, A. B.; Munoz, M. C.; Bukin, G. V.; Levchenko, G.; Real, J. A. *Adv. Mater.* **2005**, *17*, 2949–2953.
(28) Coronado, E.; Galan-Mascaros, J. R.; Gomez-Garcia, C. J.; Murcia-Martinez, A. *Chem.—Eur. J.* **2006**, *12*, 3484–3492.
(29) Gruselle, M.; Train, C.; Boubekeur, K.; Gredin, P.; Ovanesyan, N. *Coord. Chem. Rev.* **2006**, *250*, 2491–2500.
(30) Ohkoshi, S.; Ikeda, S.; Hozumi, T.; Kashiwagi, T.; Hashimoto, K. *J. Am. Chem. Soc.* **2006**, *128*, 5320–5321.
(31) Ohkoshi, S.; Tokoro, H.; Hozumi, T.; Zhang, Y.; Hashimoto, K.; Mathoniere, C.; Bord, I.; Rombaut, G.; Verelst, M.; Moulin, C. C. D.; Villain, F. *J. Am. Chem. Soc.* **2006**, *128*, 270–277.
(32) Kaneko, W.; Ohba, M.; Kitagawa, S. *J. Am. Chem. Soc.* **2007**, *129*, 13706–13712.
(33) Ohkoshi, S.; Tokoro, H.; Matsuda, T.; Takahashi, H.; Irie, H.; Hashimoto, K. *Angew. Chem., Int. Ed.* **2007**, *46*, 3238–3241.
(34) Sato, O.; Tao, J.; Zhang, Y. Z. *Angew. Chem., Int. Ed.* **2007**, *46*, 2152–2187.
(35) Chelebaeva, E.; Larionova, J.; Guari, Y.; Ferreira, R. A. S.; Carlos, L. D.; Paz, F. A. A.; Trifonov, A.; Guerin, C. *Inorg. Chem.* **2008**, *47*, 775–777.
(36) Ohba, M.; Kaneko, W.; Kitagawa, S.; Maeda, T.; Mito, M. *J. Am. Chem. Soc.* **2008**, *130*, 4475–4484.
(37) Yamada, S.; Kuwabara, K.; Koumoto, K. *Mater. Sci. Eng. B: Solid* **1997**, *49*, 89–94.
(38) Moulik, S. P.; De, G. C.; Panda, A. K.; Bhowmik, B. B.; Das, A. R. *Langmuir* **1999**, *15*, 8361–8367.
(39) Vaucher, S.; Li, M.; Mann, S. *Angew. Chem., Int. Ed.* **2000**, *39*, 1793–1796.
(40) Vaucher, S.; Fielden, J.; Li, M.; Dujardin, E.; Mann, S. *Nano Lett.* **2002**, *2*, 225–229.
(41) Catala, L.; Gacoin, T.; Boilot, J. P.; Riviere, E.; Paulsen, C.; Lhotel, E.; Mallah, T. *Adv. Mater.* **2003**, *15*, 826–829.
(42) Dominguez-Vera, J. M.; Colacio, E. *Inorg. Chem.* **2003**, *42*, 6983–6985.
(43) Moore, J. G.; Lochner, E. J.; Ramsey, C.; Dalal, N. S.; Stiegman, A. E. *Angew. Chem., Int. Ed.* **2003**, *42*, 2741–2743.
(44) Uemura, T.; Kitagawa, S. *J. Am. Chem. Soc.* **2003**, *125*, 7814–7815.
(45) DeLongchamp, D. M.; Hammond, P. T. *Chem. Mater.* **2004**, *16*, 4799–4805.
(46) DeLongchamp, D. M.; Hammond, P. T. *Adv. Funct. Mater.* **2004**, *14*, 224–232.
(47) Dujardin, E.; Mann, S. *Adv. Mater.* **2004**, *16*, 1125–1129.
(48) Yamada, M.; Arai, M.; Kurihara, M.; Sakamoto, M.; Miyake, M. *J. Am. Chem. Soc.* **2004**, *126*, 9482–9483.
(49) Cao, M. H.; Wu, X. L.; He, X. Y.; Hu, C. W. *Chem. Commun.* **2005**, 2241–2243.
(50) Catala, L.; Mathoniere, C.; Gloter, A.; Stephan, O.; Gacoin, T.; Boilot, J. P.; Mallah, T. *Chem. Commun.* **2005**, 746–748.
(51) Clavel, G.; Guari, Y.; Larionova, J.; Guerin, C. *New J. Chem.* **2005**, *29*, 275–279.
(52) Kondo, N.; Kurihara, M.; Yamada, M.; Miyake, M.; Nishijima, M.; Ohsuna, T.; Mizukami, F.; Sakamoto, M. *Chem. Lett.* **2005**, *34*, 590–591.
(53) Uemura, T.; Kitagawa, S. *Chem. Lett.* **2005**, *34*, 132–137.
(54) Brinzei, D.; Catala, L.; Louvain, N.; Rogez, G.; Stephan, O.; Gloter, A.; Mallah, T. *J. Mater. Chem.* **2006**, *16*, 2593–2599.
(55) Catala, L.; Gloter, A.; Stephan, O.; Rogez, G.; Mallah, T. *Chem. Commun.* **2006**, 1018–1020.
(56) Clavel, G.; Larionova, J.; Guari, Y.; Guerin, C. *Chem.—Eur. J.* **2006**, *12*, 3798–3804.
(57) Cobo, S.; Molnar, G.; Real, J. A.; Bousseksou, A. *Angew. Chem., Int. Ed.* **2006**, *45*, 5786–5789.
(58) Folch, B.; Larionova, J.; Guari, Y.; Datas, L.; Guerin, C. *J. Mater. Chem.* **2006**, *16*, 4435–4442.
(59) Kondo, N.; Nakajima, A.; Sasaki, Y.; Kurihara, M.; Yamada, M.; Miyake, M.; Mizukami, F.; Sakamoto, M. *Chem. Lett.* **2006**, *35*, 1302–1303.
(60) Kosaka, W.; Tozawa, M.; Hashimoto, K.; Ohkoshi, S. I. *Inorg. Chem. Commun.* **2006**, *9*, 920–922.
(61) Baioni, A. P.; Vidotti, M.; Fiorito, P. A.; Ponzio, E. A.; de Torresi, S. I. C. *Langmuir* **2007**, *23*, 6796–6800.
(62) Brinzei, D.; Catala, L.; Mathoniere, C.; Wernsdorfer, W.; Gloter, A.; Stephan, O.; Mallah, T. *J. Am. Chem. Soc.* **2007**, *129*, 3778–3779.
(63) Coronado, E.; Galan-Mascaros, J. R.; Monrabal-Capilla, M.; Garcia-Martinez, J.; Pardo-Ibanez, P. *Adv. Mater.* **2007**, *19*, 1359–1361.
(64) Molnar, G.; Cobo, S.; Real, J. A.; Carcenac, F.; Daran, E.; Vien, C.; Bousseksou, A. *Adv. Mater.* **2007**, *19*, 2163–2167.
(65) Yao, J. L.; Xu, Y.; Xue, D. S. *Chem. Phys. Lett.* **2007**, *435*, 317–321.
(66) Pajerowski, D. M.; Frye, F. A.; Talham, D. R.; Meisel, M. W. *New J. Phys.* **2007**, *9*, 1–10.
(67) Frye, F. A.; Pajerowsk, D. M.; Anderson, N. E.; Long, J.; Park, J. H.; Meisel, M. W.; Talham, D. R. *Polyhedron* **2007**, *26*, 2273–2275.
(68) Arai, M.; Miyake, M.; Yamada, M. *J. Phys. Chem. C* **2008**, *112*, 1953–1962.
(69) Boldog, I.; Gaspar, A. B.; Martinez, V.; Pardo-Ibanez, P.; Ksenofontov, V.; Bhattacharjee, A.; Gütlich, P.; Real, J. A. *Angew. Chem., Int. Ed.* **2008**, *47*, 6433–6437.
(70) Clemente-León, M.; Coronado, E.; Lopez-Munoz, A.; Repetto, D.; Brinzei, D.; Catala, L.; Mallah, T. *Chem. Mater.* **2008**, *20*, 4642–4652.
(71) Fleury, B.; Volatron, F.; Catala, L.; Brinzei, D.; Rivire, E.; Huc, V.; David, C.; Miserque, F.; Rogez, G.; Baraton, L.; Palacin, S.; Mallah, T. *Inorg. Chem.* **2008**, *47*, 1898–1900.
(72) Folch, B.; Guari, Y.; Larionova, J.; Luna, C.; Sangregorio, C.; Innocenti, C.; Caneschi, A.; Guerin, C. *New J. Chem.* **2008**, *32*, 273–282.
(73) Forestier, T.; Mornet, S.; Daro, N.; Nishihara, T.; Mouri, S.-I.; Tanaka, K.; Fouché, O.; Freysz, E.; Létard, J.-F. *Chem. Commun.* **2008**, DOI: 10.1039/b806347h.
(74) Guari, Y.; Larionova, J.; Corti, M.; Lascialfari, A.; Marinone, M.; Poletti, G.; Molvinger, K.; Guerin, C. *J. Chem. Soc., Dalton Trans.* **2008**, 3658–3660.
(75) Imaz, I.; Maspoch, D.; Rodriguez-Blanco, C.; Perez-Falcon, J. M.; Campo, J.; Ruiz-Molina, D. *Angew. Chem., Int. Ed.* **2008**, *47*, 1857–1860.
(76) Kerbellec, N.; Catala, L.; Daiguebonne, C.; Gloter, A.; Stephan, O.; Bunzli, J. C.; Guillou, O.; Mallah, T. *New J. Chem.* **2008**, *32*, 584–587.
(77) Volatron, F.; Catala, L.; Riviere, E.; Gloter, A.; Stephan, O.; Mallah, T. *Inorg. Chem.* **2008**, *47*, 6584–6586.
(78) Rieter, W. J.; Taylor, K. M. L.; An, H. Y.; Lin, W. L.; Lin, W. B. *J. Am. Chem. Soc.* **2006**, *128*, 9024–9025.

substitution reaction for a given pair of complex and BL may allow fine control of the characteristics (size, shape, surface state, etc.) of the nanoparticles and thus of their physical behavior.

Type II: CNPs include objects where coordination bonds spread only in one or two dimensions and weaker interactions operate in the remaining direction.[63,75,79] This difference in the bond strength (coordination vs hydrogen bonds, electrostatic interactions, and $\pi-\pi$ stacking) may influence the nucleation and growth processes and allow control of the particles' shapes. Nanorods or nanoplatelets may thus be prepared.

Type III: CNPs have no extended coordination bonds; they are made from the aggregation of discrete coordination complexes where only relatively weak intermolecular interactions (hydrogen bonds, $\pi-\pi$ stacking, and electrostatic) are responsible for their stability. To the best of our knowledge, two examples of this class of CNPs were reported by precipitation in a poor solvent, leading in one case to sub-50-nm objects.[80,81] The preparation of these types of nanoparticles may be of importance in the field of spin-crossover complexes in the perspective of providing bistable objects at the nanoscale. Indeed, in most spin-crossover systems, the cooperative behavior is the result of long-range interactions (elastic forces) that can be mediated by hydrogen bonds or $\pi-\pi$ stacking between the molecules within the crystal.

Reported type I and II CNPs are obtained using the classical chemical techniques that allow confinement of the growth of the objects, while type III particles are only prepared by their precipitation in a poor solvent, even though the use of inorganic matrices (SiO_2 for example) may be envisaged.

A unique feature of CNP is the possibility of preparing ordered bimetallic objects when one of the building blocks is a complex that plays the role of a ligand. In such a case, the synergy between the two different metal ions may induce a new behavior. Cyanometallates are the archetype of such building blocks. In this paper, we report our recent results on the preparation and characterization of a series of type I CNPs and we focus on their physical behavior (superparamagnetism, photomagnetism, spin crossover, and luminescence), which may be the origin of useful functionality (information storage, sensors, and labels) at the nanoscale.

Bistability is a necessary requirement for a material in the perspective of the design of a device for information storage. One of the challenges is to design bistable objects with a size as reduced as possible if high-density data storage is targeted. Bistability is expressed by the occurrence of a hysteresis loop, which is generally the result of a collective behavior, as in ferromagnets, for example.[82] However, a hysteresis loop (magnetization vs field) may be the result of the slow relaxation of the magnetization in nanoparticles due to magnetic anisotropy. A hysteresis loop may be induced by light irradiation, as in photomagnetic nanoparticles. Unfortunately, the bistability occurs in these cases at very low temperatures. In spin-crossover systems, the hysteresis loop may be centered at room temperature with a width large enough to envisage practical applications.[63]

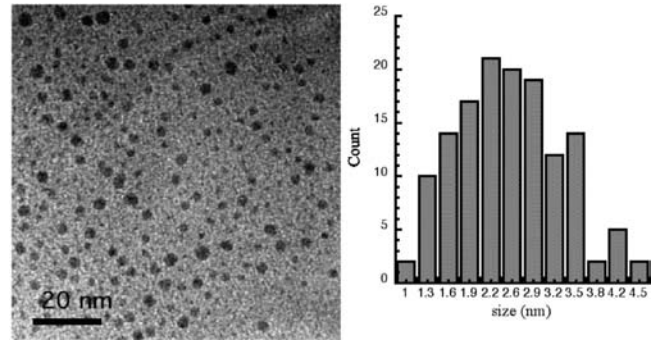

Figure 1. TEM image of $Ni[Cr(CN)_6]_{2/3}$ nanoparticles and size distribution.

Bimetallic Superparamagnetic CNPs

The archetypes of bimetallic type I CNP are those based on the Prussian blue analogue (PBA) networks; they are obtained from the reaction of a hexacyanometallate and a hexaaquo metal complex. PBA are bimetallic extended networks with a face-centered-cubic (fcc) structure. Because of the charge difference between the two components [$M(CN)_6^{3-}$ and $M'(H_2O)_6^{2+}$], the fcc neutral network has $M(CN)_6^{3-}$ vacancies. The presence of an alkali ion with adequate size to fit into the tetrahedral sites of the network (Cs^+ or Rb^+) may decrease the number of vacancies and in some cases suppress them; in such a case, the stoichiometric compounds of formula $A^I[M'^{II}M^{III}(CN)_6]$ are obtained.[83,84] The first reports aimed at the preparation of nanoparticles of PBA were made by Yamada et al. in 1997 and then by Moulik et al. in 1999.[37,38] An excellent control on the size and dispersity of the PBA was achieved by Mann and coworkers using microemulsion to control the growth of the particles.[39,40] However, the recovery of the particles from the microemulsion was not reported.

Because of the low metal density due to the coordination nature of the nanoparticles, objects with a magnetic moment intermediate between that of the largest molecules and of the smallest oxide or metallic particles can be prepared. In order to investigate the magnetic behavior of a small assembly of such objects or that of a single nanoparticle and

(79) Jeon, Y. M.; Heo, J.; Mirkin, C. A. *J. Am. Chem. Soc.* **2007**, *129*, 7480–7481.
(80) Imaz, I.; Luis, F.; Carbonera, C.; Ruiz-Molina, D.; Maspoch, D. *Chem. Commun.* **2008**, 1202–1204.
(81) Johnson, C. A.; Sharma, S.; Subramaniam, B.; Borovik, A. S. *J. Am. Chem. Soc.* **2005**, *127*, 9698–9699.
(82) The hysteresis behavior in SMMs is assigned to single molecules as a result of a slow relaxation of the magnetization (see other papers in this issue). This is the case as well for single domain superparamagnetic nanoparticles.
(83) Mallah, T.; Ferlay, S.; Auberger, C.; Helary, C.; LHermite, F.; Ouahes, R.; Vaissermann, J.; Verdaguer, M.; Veillet, P. *Mol. Cryst. Liq. Cryst. A* **1995**, *273*, 141–151.
(84) Gadet, V.; Mallah, T.; Castro, I.; Verdaguer, M.; Veillet, P. *J. Am. Chem. Soc.* **1992**, *114*, 9213–9214.

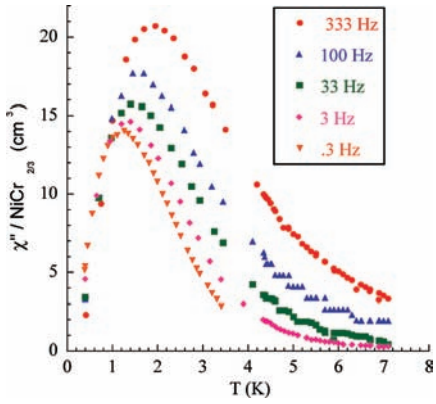

Figure 2. Thermal variation of the out-of-phase ac susceptibility for $Ni[Cr(CN)_6]_{2/3}$ nanoparticles at different frequencies of the oscillating magnetic field in zero direct current magnetic field.

to integrate them into devices, it is necessary to achieve their dispersion in solution.

We focus here on the ferromagnetic $Ni^{II}Cr^{III}$ PBA analogue. The microemulsion technique allowed the stabilization of neutral 3 nm particles of formula $Ni[Cr(CN)_6]_{2/3}$ (Figure 1). Recovery of the particles was achieved by adding *p*-nitrobenzylpyridine to the microemulsion.[41] The powder was then redispersed in a solution containing dichloromethane and a small amount of *N*,*N*-dimethylformamide (DMF). The magnetic studies of a sample of these particles highly diluted in an organic polymer [poly(vinylpyrrolidone), PVP] matrix show a superparamagnetic behavior with a blocking temperature of 2 K. The alternating current (ac) susceptibility curves present a frequency-dependent out-of-phase component (Figure 2), leading to an anisotropy energy barrier $\Delta = 30$ K and a characteristic relaxation time τ_0 of 1.1×10^{-11}s.

Nanoparticles of Prussian blue and its analogues were subsequently prepared by different chemical techniques;[42−44,48,49,51,53−56,58,61,65−68,72,85−89] however, only in few cases was a superparamagnetic behavior observed.[55,68] This is probably due to the difficulty to reduce the interparticle dipolar interactions within the studied sample.

The introduction of an alkali ion (Cs^+), which can occupy the tetrahedral sites of the fcc structure and thus reduce the hexacyanochromate(III) vacancies, turned out to have a dramatic influence of the nucleation and growth processes of the particles. Indeed, the reaction in water of $K_3[Cr(CN)_6]$ and $NiCl_2 \cdot 6H_2O$ in the molar ratio 2:3 ($c_{Ni} = 10^{-3}$ M) without the presence of any organic or inorganic agent to confine the growth of the 3D network leads to the formation of large particles within a few minutes and finally to the precipitation of a powder. If the same molar ratio of the two components is used, particles with a size of around 15 nm are obtained. The addition of CsCl when reacting the two components affords quasi-monodisperse nanocrystals with a size of 6 nm (noted as CsNiCr in the following; Figure 3). Kinetic studies are underway to elucidate the peculiar role of the alkali on the nucleation and growth processes. The ζ potential of an as-prepared solution gives a value of −31 mV, indicating the presence of negatively charged objects.

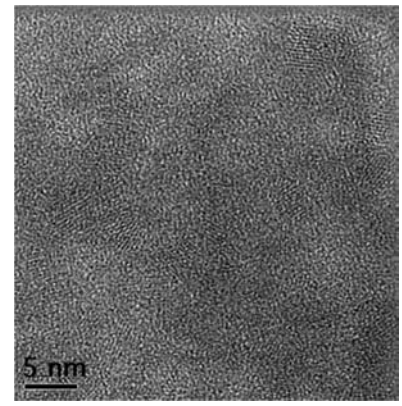

Figure 3. HRTEM micrograph of the 6 nm CsNiCr nanoparticles.

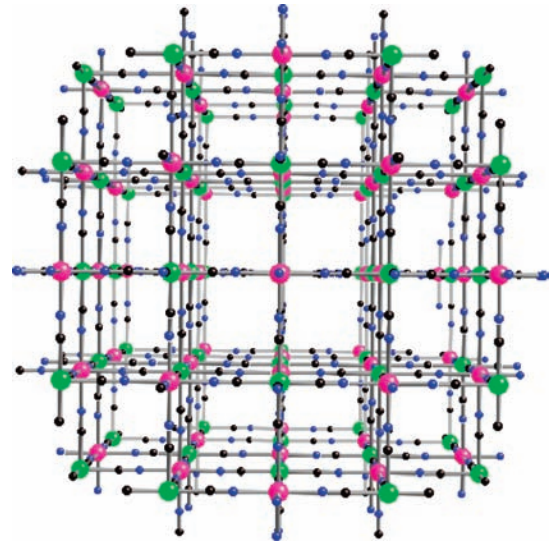

Figure 4. Schematic view of a 2 × 2 nm particle of a PBA, revealing the very low metal density (metal ions are in green and violet).

The success of the spontaneous stabilization of bare CsNiCr nanoparticles in water opens tremendous possibilities of manipulating them in solution and performing an adequate functionalization of their surface. Indeed, the surface of the bimetallic particles is made of two types of sites. One is the nitrogen atoms of the $Cr(CN)_6$ molecules, which play the role of a ligand and allow the attachment of complexes on the particle's surface, and the other is the water molecules linked to Ni^{II}, which can be substituted by other ligands (organic or a metal complex), conferring to the particles the role of a complex (Figure 4). The addition of an excess of an organic ligand [3-(pyrol-1-ylmethyl)pyridine] allows the precipitation of the particles in water. A redispersion in methanol of the as-coated particles can be achieved. The high-angle annular dark-field scanning transmission electronic microscopy (HAADF-STEM) images reveal the pres-

(85) Fiorito, P. A.; de Torresi, S. I. C. *J. Electroanal. Chem.* **2005**, *581*, 31–37.
(86) Kong, Q.; Chen, X. G.; Yao, J. L.; Xue, D. S. *Nanotechnology* **2005**, *16*, 164–168.
(87) Guari, Y.; Larionova, J.; Molvinger, K.; Folch, B.; Guerin, C. *Chem. Commun.* **2006**, 2613–2615.
(88) Gotoh, A.; Uchida, H.; Ishizaki, M.; Satoh, T.; Kaga, S.; Okamoto, S.; Ohta, M.; Sakamoto, M.; Kawamoto, T.; Tanaka, H.; Tokumoto, M.; Hara, S.; Shiozaki, H.; Yamada, M.; Miyake, M.; Kurihara, M. *Nanotechnology* **2007**, *18*, 345609–345614.
(89) Chelebaeva, E.; Guari, Y.; Larionova, J.; Trifonov, A.; Guerin, C. *Chem. Mater.* **2008**, *20*, 1367–1375.

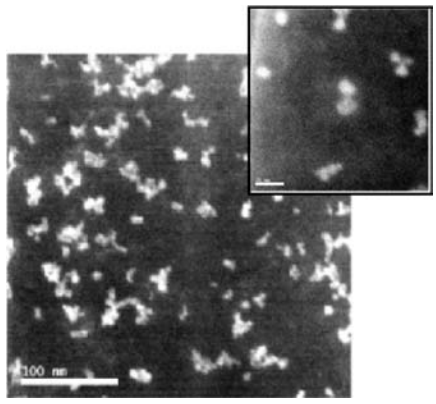

Figure 5. Dark-field STEM image of the 6 nm CsNiCr particles coated by 3-(pyrol-1-ylmethyl)pyridine (scale bar 100 nm). Inset: scale bar 20 nm.

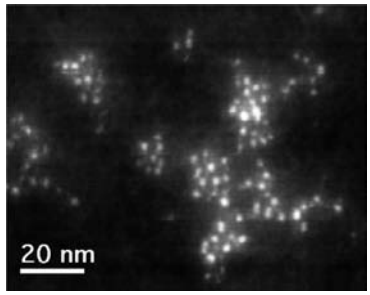

Figure 6. Dark-field STEM image of the 6 nm CsNiCr particles coated by pentadecylamine.

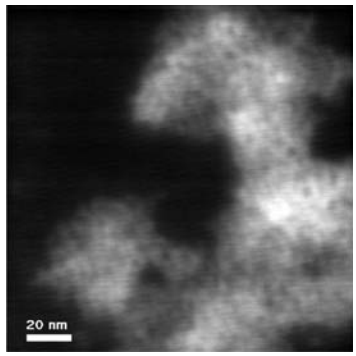

Figure 7. Dark-field STEM image of the 6 nm CsNiCr particles coated by CTA^+.

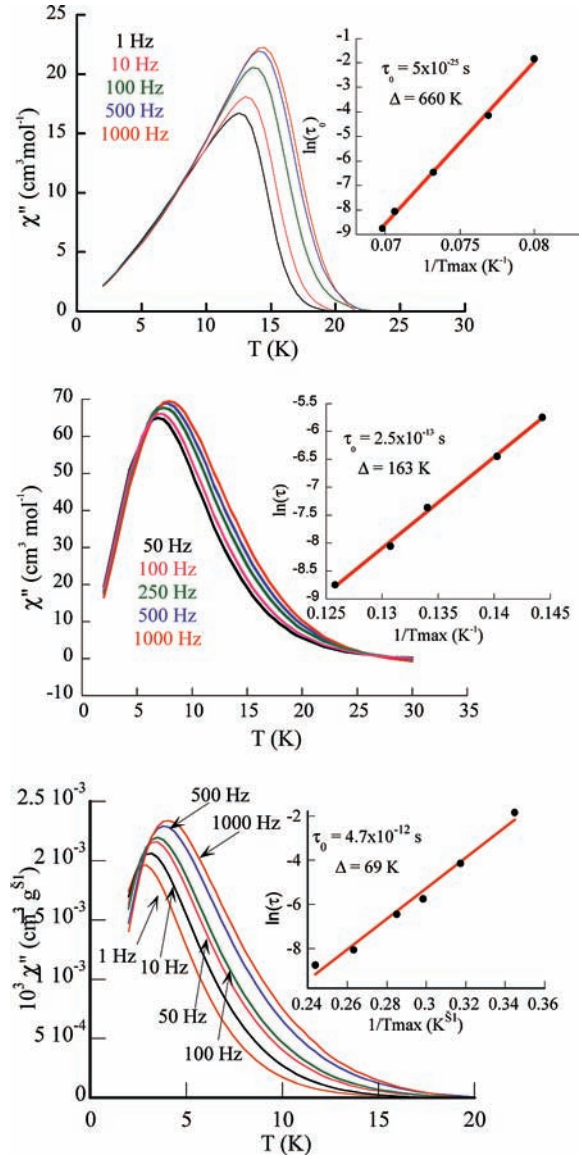

Figure 8. Thermal variation of the out-of-phase ac susceptibility at different frequencies of the oscillating magnetic field for the 6 nm CsNiCr particles coated by CTA^+ (top), diluted in PVP (10% by weight) (middle), and diluted in PVP (1% by weight) and $\ln(\tau) = f(1/T_{max})$ (inset).

ence of aggregates of about 15 nm size formed from the primary 6 nm particles (Figure 5). The use of another organic ligand with an amine group (pentadecylamine) seems to slightly affect their size because the STEM imaging reveals the presence of particles in the range 3−5 nm (Figure 6). The negative charge of the particles allows their coating by an organic cation such as cetyltrimethylammonium (CTA^+), which plays the role of surfactant. For this case, the interaction between the particles and the organic shell is electrostatic while coordination bonds are present when neutral amine or pyridine-terminated ligands were used. The STEM images confirm the presence of the particles after their redispersion in ethanol (Figure 7). However, an aggregation of the 6 nm primary particles occurs probably on the grid because of the interaction between the long hydrophobic chains of the CTA^+ cation.

The recovery of the particles achieved by the addition of an excess of cetyltrimethylammonium chloride (CTACl) to the solution allows one to obtain crucial information concerning the role of the Cs^+ cations. Because CTA^+ is a bulky cation that cannot be inserted into the tetrahedral sites of the fcc network, it will replace only the Cs^+ ions not inserted in the tetrahedral sites of the fcc structure. The elemental analysis of the precipitate obtained after the addition of an excess of CTACl to the aqueous solution containing the particles leads to the following formula: $Cs_{0.4}Ni[Cr(CN)_6](CTA)_{0.6}(H_2O)_5$. This formula gives the amount of inserted Cs^+ and confirms the negative charge of the particles that were spontaneously formed in solution.[54]

The comparison of the magnetic properties of the particles recovered with CTACl and those diluted in PVP reveals the important role of the particles' processing on their behavior. Indeed, a spin-glass-like behavior is observed for the particles coated with CTA^+ (Figure 8, top) while a nearly superparamagnetic one with a blocking temperature of 9 K (Figure 8, middle) is found for the particles diluted in PVP (10% by

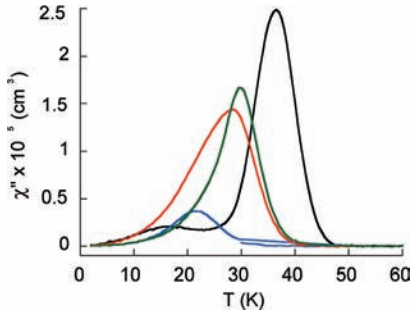

Figure 9. $\chi'' = f(T)$ for the LB films made in different conditions: at a pressure of 30 mN/m, using DODA as the surfactant and a concentration (c) of nanoparticles of 10^{-5} M(black); $c = 5 \times 10^{-6}$ M(blue); using a 1.1:1 DODA/DHP mixture of surfactant, a pressure of 30 mN/m and $c = 10^{-5}$ M(red); using a 1.1:1 DODA/DHP mixture of surfactant, a pressure of 10 mN/m and $c = 10^{-5}$ M(green).

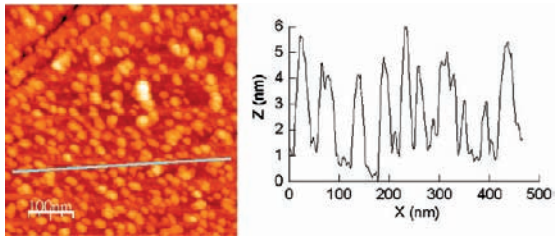

Figure 10. AFM image of a monolayer of the 6 nm CsNiCr particles anchored on a Si(100)-functionalized surface and topography along a 500 nm line.

weight). The degree of dilution in PVP affects the magnetic behavior as expected. A superparamagnetic behavior with a lower blocking temperature (T_B = 5 K) and quasi no interparticle dipolar interactions is observed (Figure 8, bottom) when the nanoparticles are highly diluted in the PVP polymer matrix (1% by weight).

Using dioctadecyldimethylammonium bromide (DODABr) instead of CTACl as a cationic surfactant allows the redispersion of the particles in different solvents (ethanol, mixture of ethanol and dichloromethane, and DMF) without the formation of large aggregates in solution, opening the possibility of their processing by the Langmuir−Blodgett (LB) technique. Multilayers of the $Cs_{0.4}Ni[Cr(CN)_6]_{0.9}^{3-}$ particles were processed, yet starting from aqueous subphases containing the CNPs. The magnetic properties of the LB films were found to be dependent on the concentration of the precursor solution, the surface pressure used to stabilize the films, and the presence of the anionic surfactant dihexadecylphosphate (DHP) that dilute the particles within the monolayers.[70] The Curie temperature of these LB films ranges from 60 K for the films prepared from the more concentrated solution to 30 K for those prepared with the diluted subphases (Figure 9).

The negative charge of the particles and the role of "ligand" that they play allow their organization as monolayers on adequately functionalized silicon, a technologically interesting surface.[71] The hydrogen-terminated Si(100) substrate was first functionalized by hydrosylilation using undecanoic acid diluted in undecene (1:100). Then, the substrate was reacted with the organic ligand *N*,*N*-bis[(pyridin-2-yl)methyl]propane-1,3-diamine, leading to the formation of an amide bond with the grafted tridentate ligand. The

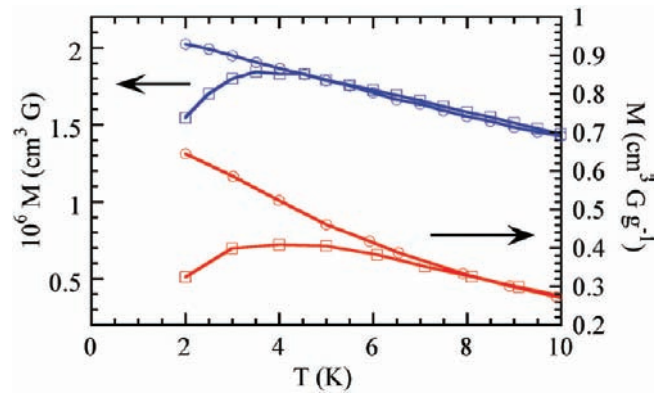

Figure 11. Field-cooled (←) and zero-field-cooled (□) magnetization plots for the CsNiCr nanoparticles diluted in PVP (red) and grafted on silicon (blue).

immersion of the as-functionalized surface in a methanolic solution of $NiCl_2 \cdot 6H_2O$ affords the $N_3Ni(H_2O)_3^{2+}$ complexes pointing out of the substrate and ready to react with the negatively charged nanoparticles. The atomic force microscopy (AFM) imaging indicates the formation of a monolayer of the CsNiCr nanoparticles as expected after dipping the substrate in the aqueous solution containing the particles (Figure 10). The investigation of the magnetic properties of the monolayer shows a superparamagnetic behavior (Figure 11) with a blocking temperature (T_B = 3.5 K) similar to that of the particles highly diluted in PVP (T_B = 4 K). The next step consists in the preparation of monolayers with different concentrations of nanoparticles in order to tune their blocking temperature and reveal the threshold where collective behavior occurs.

Photomagnetic CNPs

One of the most studied photomagnetic networks is the cobalt hexacyanoferrate Prussian blue analogue of the general formula $A_xCo_y[Fe(CN)_6]_z \cdot nH_2O$ (x, y, z being independent). Light irradiation induces the formation of the cyanide-bridged paramagnetic pair Co^{II}/Fe^{III} due to an electron transfer from ferrocyanide to the diamagnetic Co^{III}.[3,7] The preparation of nanoparticles based on this photomagnetic network using different approaches has been reported.[43,48,66,67] Talham, Meisel, and co-workers recently reported the synthesis of nanoparticles with sizes ranging from 3.3 to 13 nm using PVP to confine their growth. Upon irradiation, a paramagnetic behavior was observed for the small particles (3.3 and 6.9 nm) while a magnetic transition resulting from a long-range order occurs for the larger particles (9.7 and 13 nm).[66]

Photomagnetism was also discovered in the cyanide-bridged network based on octacyanomolybdate(IV) and Cu^{II} of formula $Cu^{II}_2Mo^{IV}(CN)_8$.[13,14] The magnetic studies of this system, before irradiation, reveal a paramagnetic behavior down to 2 K because of the absence of any measurable exchange interaction between the two $S = {}^1/_2$ Cu^{II} ions through the diamagnetic $Mo^{IV}(CN)_8$ (d^2, $S = 0$) molecules. Irradiation of the compound at 415 nm induces an electron transfer from Mo^{IV} to one of the two Cu^{II} ions, leading to the formation of $Mo^{V}-CN-Cu^{II}$ paramagnetic pairs throughout the network. The exchange interaction within this pair

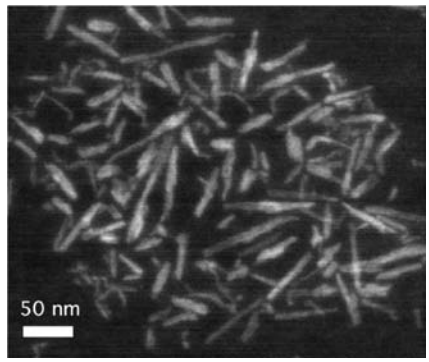

Figure 12. Dark-field STEM image of the $CuMo(CN)_8$ nanoparticles.

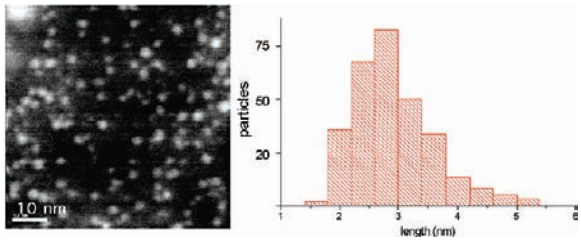

Figure 13. Dark-field STEM image of the trimetallic $NiCuMo(CN)_8$ particles and size distribution.

turns out to be ferromagnetic. Thus, irradiating the sample at low temperature (10 K) induces a conversion from the stable paramagnetic state to the metastable ferromagnetic state; the return to equilibrium is achieved by heating the sample above 200 K.

Nanorods with an aspect ratio of 0.19 ($70.3 \pm 28.8 \times 11.3 \pm 3.3$ nm) of the $Cu^{II}_2Mo^{IV}(CN)_8$ compound are obtained if the reaction between the two components is performed in water in the presence of PVP (Figure 12).[50] The origin of the formation of these anisotropic particles is under investigation. The photomagnetic behavior of the nanoparticles is similar to that of the bulk compound. However, a complete electron transfer is observed for the nanoparticles, while only a 70% transformation is usually observed in the bulk. Unfortunately, no blocking of the magnetization occurs down to $T = 2$ K. Because Cu^{II} and Mo^{IV} have an $S = {}^1/_2$, they do not possess a magnetic anisotropy (no zero-field splitting); we reasoned that the introduction of a metal ion possessing a large magnetic anisotropy may induce the blocking of the magnetization within the nanoparticles. The same reaction that led to the formation of the 70×11 nm nanoparticles described above was carried out by introducing the same amount of the three components Ni^{II}, Cu^{II}, and $Mo(CN)_8^{4-}$, leading to a powder with the unit formula $NiCuMo(CN)_8$ as expected.[62] The STEM imaging of a drop of the solution casted on a TEM grid reveals the formation of spherical objects (2.9 ± 0.7 nm) (Figure 13). A striking result is the very small size of the particles, which is due to the introduction of Ni^{II}. We have already observed this size effect for the Prussian blue analogues, which is suspected to be due to the weaker lability of Ni^{II} in water in comparison to Cu^{II}. Kinetics studies are underway in order to understand the role of Ni^{II} in the first stage of the formation of the nanoparticles.

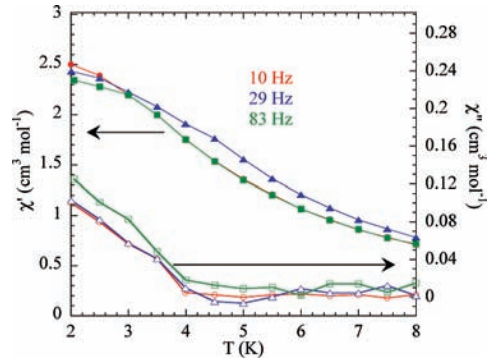

Figure 14. Thermal variation of the in-phase and out-of-phase magnetic susceptibilities for the 3 nm trimetallic $NiCuMo(CN)_8$ nanoparticles.

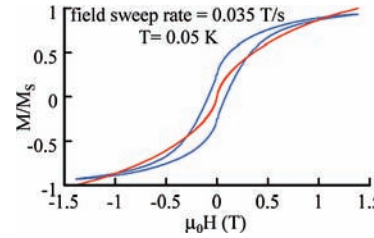

Figure 15. Reduced magnetization vs magnetic field for the 3 nm trimetallic $NiCuMo(CN)_8$ nanoparticles before (red) and after irradiation (blue) at $T = 0.05$ K.

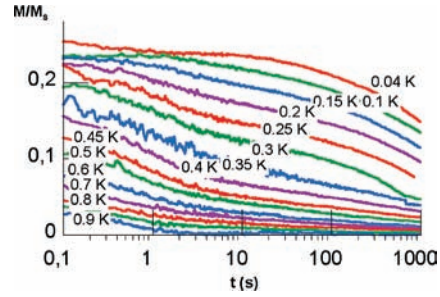

Figure 16. Plots of the decay of the magnetization between $T = 1$ and 0.04 K for the 3 nm trimetallic $NiCuMo(CN)_8$ nanoparticles.

Frequency-dependent ac susceptibility studies were performed after irradiation of a sample of the nanoparticles at 415 nm in a SQUID magnetometer. An out-of-phase signal was detected below $T = 4$ K, indicating the possibility of a blocking of the magnetization (Figure 14). In order to confirm this result, a micrometric portion of a PVP film containing the particles was studied in the 0.05−5 K range using a microSQUID.[62] As expected, at $T = 0.05$ K, no hysteresis was observed before irradiation (Figure 15). The irradiation performed with a blue-light diode (405 nm; power ~ 1 mW/cm^2) over 5 h leads to the opening of a hysteresis loop, with a coercive field of 920 Oe (Figure 15). Relaxation measurements were performed in order to ensure that the opening of the hysteresis loop is due to the blocking of the magnetization and not to a collective behavior as a result of interparticle dipolar interactions: at a given temperature, the magnetization was first saturated, the magnetic field was swept down to zero (at 0.14 T/s), and the magnetization decay was then measured at different temperatures as a function of time (Figure 16). The thermal dependence of the relaxation time τ (extracted from a scaling process) revealed two regimes (Figure 17). A temperature-activated regime is

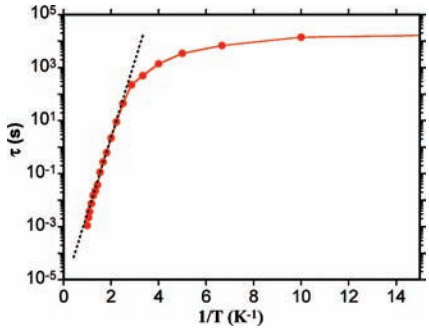

Figure 17. Variation of the relaxation time (τ) of the magnetization vs $1/T$ for the 3 nm trimetallic $NiCuMo(CN)_8$ nanoparticles.

observed for $T > 0.3$ K, which allows one to extract the effective energy barrier at zero field ($\Delta = 6.7$ K) and the attempt time ($\tau_0 = 3 \times 10^{-6}$ s) corresponding to the Arrhenius law $\tau = \tau_0 \exp(\Delta/T)$. The large τ_0 value corresponds to what is expected for superparamagnetic single-domain objects.[90] Below 0.3 K, a temperature-independent regime was observed, suggesting the occurrence of quantum magnetic tunneling. This behavior is similar to that observed in many single-molecule magnets.[91] Indeed, these 3 nm coordination particles can be described as giant clusters of about 55 ± 8 $Ni^{II}Cu^{I}Mo^{V}$ units ($S_{max} = 82 \pm 12$). The absence of steps in the hysteresis loop, which is the signature of quantum tunneling of the magnetization, may be due to the relatively large size of the particles in comparison to molecules or probably to the fact that all of the objects under investigation do not have strictly the same size and thus the same behavior.

This is the first example of light-induced blocking of the magnetization in a molecule-based nanoobject. Introduction of other anisotropic ions like Co^{II} and a slight increase of the size of the nanoparticle should shift the blocking temperature upward.

Spin-Crossover CNPs

Spin-crossover systems are among the most interesting molecular materials because thermal hysteresis centered at room temperature has been reported in many cases.[4,12,27,92]However, even though the spin change occurs in isolated molecules, the hysteresis (and thus bistability) is a cooperative phenomenon. In order to take advantage of the interesting properties of these systems, the objects must be as small as possible and retain the bistable behavior. An important step toward this goal has recently been achieved.[57,63,64,69,73,77]

Beyond the perspective of applications, one important issue in spin-crossover systems is to gain insight into the effect of size reduction on the collective behavior responsible for the hysteresis loop. Is it possible to reduce the grain size at the nanometric scale keeping the hysteresis loop? What is this ultimate size? Coronado et al. showed that 10 nm particles of the 1D $[Fe(Htrz)_2(trz)](BF_4)$] (where Htrz is triazole) material still possess the bistable properties of the bulk, i.e., a quasi-square thermal hysteresis near room temperature (at $T = 360$ K) with a width of 40 K. This bistability opens the possibility of storing information in these nanoparticles. In our group, we focused on the 3D Hoffmann clathrate $[Fe(pyrazine)Pt(CN)_4]\cdot 2H_2O$ discovered by Real and co-workers,[12] particularly on preparing and investigating the magnetic behavior of nanoparticles with different sizes.

The $[Fe(pyrazine)Pt(CN)_4]\cdot 2H_2O$ structure is made from 2D cyanide-bridged layers where each $Pt(CN)_4$ molecule is surrounded by four Fe^{II} ions and each Fe^{II} ion by four $Pt(CN)_4$ molecules; the layers are linked together by pyrazine ligands that occupy the apical position of the Fe atoms. Water molecules are present within the 3D network and have an important influence on the magnetic behavior. Real et al. showed that removing the water molecules by heating the sample at 140 °C leads to a material exhibiting a quasi-square hysteresis loop centered at $T = 290$ K.

We used reversed micelles to prepare nanoparticles of this material and showed that particles' sizes may be tuned by the concentration of the metal ions.[77] Three different concentrations of the metal ions, namely, 0.14, 0.08, and 0.02 mol/L were used, leading to samples containing 7, 14, and above 40 nm particles, respectively (Figure 18). The higher concentration affords the smallest particles, as expected from a nucleation-controlled process. The transmission electron microscopy (TEM) imaging shows a large size distribution for the largest particles, while quasi-monodisperse objects were obtained for the other two cases [7.7 nm ($\sigma = 1.2$) and 14.7 nm ($\sigma = 2.3$) × 12.1 nm ($\sigma = 2.1$)].[77] We focus in the following on the two latter samples. The particles were recovered from the microemulsions by the addition of *p*-nitrobenzylpyridine; the flocculate was centrifuged, washed with acetone, and dried under vacuum. The X-ray powder diffraction (XRPD) diagrams of the samples correspond well to what is expected for the bulk (Figure 19). Using Scherrer's equation on single peaks gives the expected size of 7 and 14 nm for the samples obtained by using the 0.14 and 0.08 mol/L concentrations, respectively. Redispersion of the 14 nm particles was possible in DMF. However, the redispersion alters somehow the shape of the particles because less faceted objects are imaged (Figure 20).

Prior to the magnetic studies, the samples were heated to 140 °C for 4 h in order to remove the crystallization water molecules as for the bulk compound. We checked that the heating process did not alter the structural integrity of the nanoparticles. The particles have a different magnetic behavior than the bulk, as shown from the $\chi_M T = f(T)$ plots (Figure 21). The size reduction leads to three effects: (i) the transition is less abrupt, (ii) the hysteresis is narrower and almost disappears for the 7 nm particles, and (iii) the transition temperature shifts downward. Another consequence of the size reduction is the incompleteness of the transition at low temperature. The $\chi_M T$ values for the 14 and 7 nm samples are equal to 1.6 and 1.2 $cm^3/mol\cdot K$, respectively, which correspond to low-temperature-remaining high-spin (HS) fractions of 34 and 45%, respectively.

(90) Dormann, J. L.; Fiorani, D. *J. Magn. Magn. Mater.* **1995**, *140*, 415–418.
(91) Gatteschi, D.; Sessoli, R. *Angew. Chem., Int. Ed.* **2003**, *42*, 268–297.
(92) Krober, J.; Codjovi, E.; Kahn, O.; Groliere, F.; Jay, C. *J. Am. Chem. Soc.* **1993**, *115*, 9810–9811.

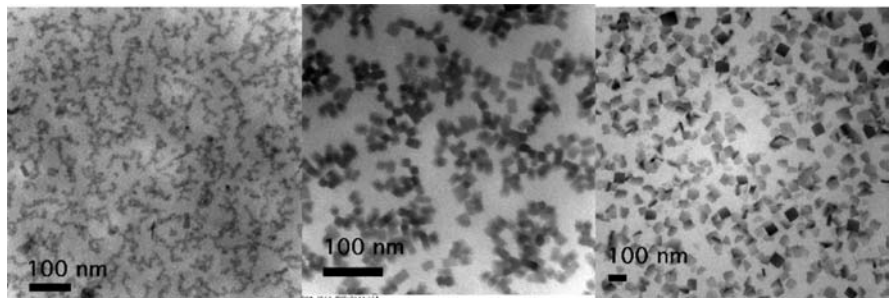

Figure 18. TEM images of three different preparations of the Fe(pyrazine)Pt(CN)$_4$ nanoparticles.

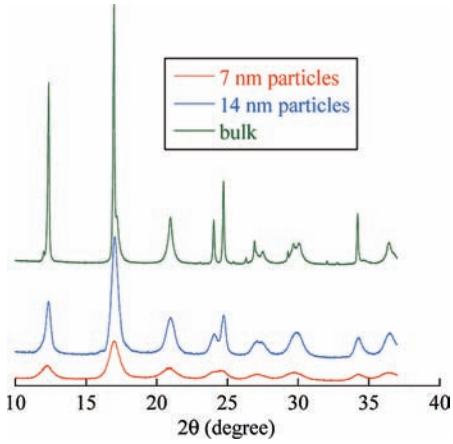

Figure 19. XRPD diagrams of the 7 and 14 nm particles and the bulk Fe(pyrazine)Pt(CN)$_4$ compound.

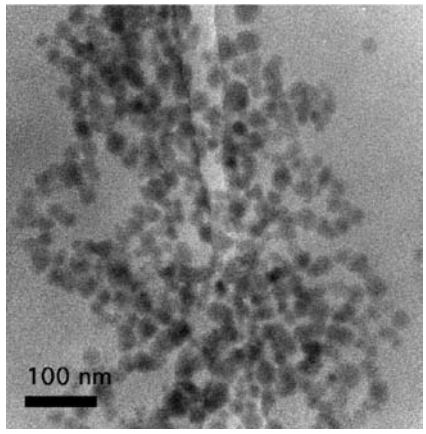

Figure 20. TEM image of the 14 nm Fe(pyrazine)Pt(CN)$_4$ particles dispersed in DMF.

The smallest particles possess the largest residual HS sites, which correspond to what is expected from the surface effect assuming that part or all of the peripheral complexes remain in the HS state. A more quantitative analysis needs further information on the thickness of the particles. The TEM imaging of the largest particles (Figure 18c) indicates a platelet like shape with a thickness much smaller than those for the two other directions. Further electronic microscopy investigations are planned in order to determine accurately the thickness of the platelets. In parallel, Mössbauer studies are underway to quantify the HS and low-spin (LS) fractions at different temperatures.

The interesting feature of the magnetic behavior of the 14 nm particles is the presence of a hysteresis of 6.1 K ($T_{c1}\downarrow$ = 262.1 K and $T_{c2}\uparrow$ = 268.2 K) despite the relatively smooth transition. Usually, a hysteresis loop in spin-crossover

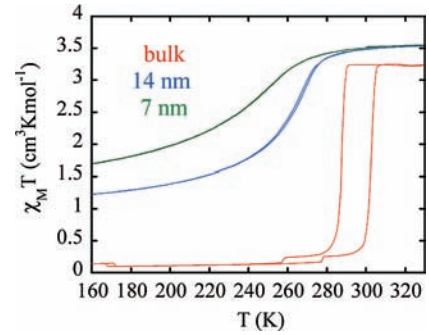

Figure 21. Thermal variation of the $\chi_M T$ product for the particles and the bulk Fe(pyrazine)Pt(CN)$_4$ compound.

compounds occurs only for an abrupt transition. Furthermore, dilution studies on the [Fe(pyrazine)Pt(CN)$_4$] bulk compound (replacing Fe^{II} by Ni^{II} or Co^{II}) shows that the hysteresis loop disappears well before the transition becomes as smooth as that observed for the 14 nm nanoparticles.[93] Our hypothesis is that each particle in the sample has an abrupt transition with a given hysteresis loop but, because of the size distribution, each particle has a different transition temperature and a different loop width; the largest particles have the highest transition temperatures and the largest loop widths. Thus, because of the size distribution, a given sample presents a smooth $\chi T = f(T)$ curve but with a hysteresis loop due to the superposition of different transition temperatures and different loop widths. This hypothesis is supported by the fact that the sample with particles' sizes centered at 7 nm has indeed a lower transition temperature with almost no hysteresis. The preparation of samples with different particles' sizes and the investigation of the physical behavior of an assembly of well-isolated particles and that of a single particle is necessary, on the one hand, to confirm our assumption and, on the other hand, to determine the size below which bistability is still present.[94]

Lanthanide-Containing Luminescent CNPs

Nanoparticles containing lanthanide ions (oxides, phosphates, and fluorides) have first been developed using synthetic strategies inspired by the work on quantum dots

(93) Tayagaki, T.; Galet, A.; Molnar, G.; Munoz, M. C.; Zwick, A.; Tanaka, K.; Real, J. A.; Bousseksou, A. *J. Phys. Chem. B* **2005**, *109*, 14859–14867.

(94) While this paper was in the review process, a report on nanoparticles based on the same network but with larger sizes (230 and 60 nm) appeared in the literature (see ref 69).

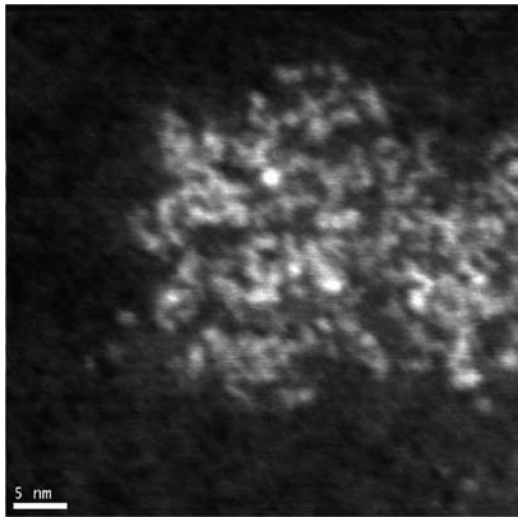

Figure 22. Dark-field STEM image of the $Tb_2bdc_3(H_2O)_4$ nanoparticles.

carried out in nonaqueous media.[95−100] The stabilization of luminescent nanoparticles in aqueous media is necessary for applications in biology. Aqueous procedures involving a luminescent core and different shells allowing an adequate functionalization of doped vanadate and phosphate nanoparticles were recently reported.[101]

CNPs offer a very interesting alternative because infinite possibilities for the synthesis of nanoobjects containing lanthanides are available, limited only by the number of coordination networks one may be able to prepare. The first sub-10-nm luminescent nanoparticles based on a coordination network were prepared by confining the growth (PVP) of the 3D network $Tb_2(bdc)_3(H_2O)_4$ (H_2bdc is 1,4-benzenedicarboxylic) already reported by Yaghi et al. in 1999.[102] Luminescent CNPs have the following advantages: (i) they can be prepared at room temperature, (ii) their synthesis can be achieved in a single step, (iii) they may be soluble in water, and (iv) their size may be tuned and controlled to less than a few nanometers, allowing different applications in biology.[103,104] A white powder is obtained by adding acetone to an aqueous solution containing a stoichiometric amount of Na_2bdc and $TbCl_3 \cdot 6H_2O$ in the presence of PVP.[76] Standard characterization (infrared and XRPD) of the white powder confirmed the presence of objects possessing the same structure as the parent 3D compound.[105] STEM-HAADF images obtained with a spatial resolution of 0.8 nm (Figure 22) allow identification of assemblies of particles within PVP with a size of around 4 nm. The presence of a relatively large amount of PVP with respect to terbium limits the observation of well-defined objects. Electron energy loss spectroscopy was carried out and demonstrates that the contrast observed on the images is due to the terbium nanoparticles.[76] The typical length of a particle was estimated on the profile of STEM-HAADF images, and an average of 3.1 nm with a standard deviation of 0.5 nm was found (from a sparse statistic of 32 particles).

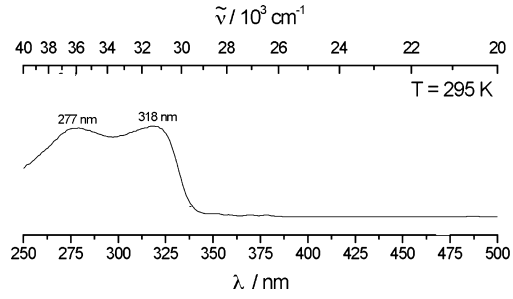

Figure 23. Excitation spectrum of the terbium-containing nanoparticles.

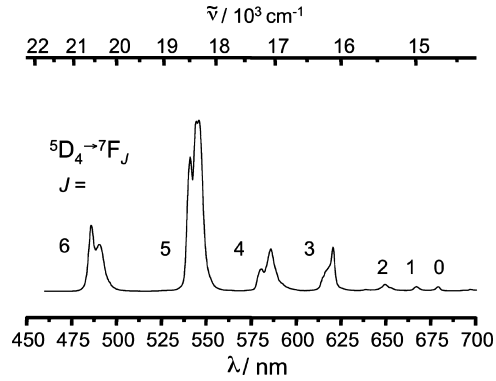

Figure 24. Emission spectrum of the terbium-containing nanoparticles.

The luminescent behavior of the terbium-containing nanoparticles was investigated on a dispersion of the sample in water under excitation at $\lambda = 312$ nm (Figure 23). The characteristic $^5D_4 \rightarrow {}^7F_J$ transitions are detected in the visible range between 490 and 680 nm, with the hypersensitive $^5D_4 \rightarrow {}^7F_5$ transition (546 nm) being the most intense (Figure 24). The quantum yield of the nanoparticles determined by Wrighton's method amounts to $26.3 \pm 2.2\%$ and the terbium ($^5D_4$) lifetime is equal 0.87 ± 0.05 ms.[106] The luminescence decay of the excited states is single exponential with a unique lifetime, which suggests that the Tb ions of the nanoparticles including those belonging to the surface (almost 50% for a 4−5 nm particle) all have a unique environment. The outer coordination sphere of the Tb ions is thus occupied by the carboxylic ligand as in the core and not by water molecules or by the donor atoms of the pyrrolidone group of PVP.

(95) Smets, B. M. J. *Mater. Chem. Phys.* **1987**, *16*, 283–299.
(96) Riwotzki, K.; Haase, M. *J. Phys. Chem. B* **1998**, *102*, 10129–10135.
(97) Riwotzki, K.; Meyssamy, H.; Schnablegger, H.; Kornowski, A.; Haase, M. *Angew. Chem., Int. Ed.* **2001**, *40*, 573–576.
(98) Stouwdam, J. W.; van Veggel, F. C. J. M. *Nano Lett.* **2002**, *2*, 733–737.
(99) Lehmann, O.; Meyssamy, H.; Kompe, K.; Schnablegger, H.; Haase, M. *J. Phys. Chem. B* **2003**, *107*, 7449–7453.
(100) Bazzi, R.; Flores, M. A.; Louis, C.; Lebbou, K.; Zhang, W.; Dujardin, C.; Roux, S.; Mercier, B.; Ledoux, G.; Bernstein, E.; Perriat, P.; Tillement, O. *J. Colloid Interface Sci.* **2004**, *273*, 191–197.
(101) Buissette, V.; Giaume, D.; Gacoin, T.; Boilot, J. P. *J. Mater. Chem.* **2006**, *16*, 529–539.
(102) Reineke, T. M.; Eddaoudi, M.; Fehr, M.; Kelley, D.; Yaghi, O. M. *J. Am. Chem. Soc.* **1999**, *121*, 1651–1657.
(103) Beaurepaire, E.; Buissette, V.; Sauviat, M. P.; Giaume, D.; Lahlil, K.; Mercuri, A.; Casanova, D.; Huignard, A.; Martin, J. L.; Gacoin, T.; Boilot, J. P.; Alexandrou, A. *Nano Lett.* **2004**, *4*, 2079–2083.
(104) Casanova, D.; Giaume, D.; Gacoin, T.; Boilot, J. P.; Alexandrou, A. *Biophys. J.* **2007**, 654A–655A.
(105) Daiguebonne, C.; Kerbellec, N.; Guillou, O.; Bunzli, J. C.; Gumy, F.; Catala, L.; Mallah, T.; Audebrand, N.; Gerault, Y.; Bernot, K.; Calvez, G. *Inorg. Chem.* **2008**, *47*, 3700–3708.
(106) Wrighton, M. S.; Ginley, D. S.; Morse, D. L. *J. Phys. Chem.* **1974**, *78*, 2229–2233.

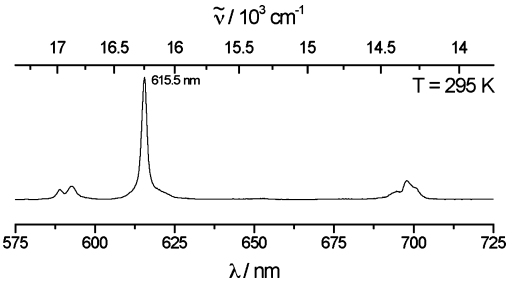

Figure 25. Emission spectrum of the europium-containing nanoparticles.

The europium-containing nanoparticles were prepared by the same procedure. They present the expected luminescent behavior with an intense band at 615.5 nm (red) upon excitation at $\lambda = 312$ nm (Figure 25). The lifetime of the europium-containing particles (0.37 ± 0.01 ms) was found to be similar to that of the bulk compound (0.47 ± 0.02 ms).

The emission spectra of the nanoparticles were carried out every 1 h for 20 h without any change, which is consistent with a very good stability of the objects in solution. These results open the perspective of a room-temperature one-step route to a large variety of luminescent nanoparticles in which chemists can control the spacing between the metal ions using adapted organic ligands.

Conclusion

One important issue is the organization of the CNPs in two dimension (on surfaces) or as crystals. The organization of the superparamagnetic objects as monolayers and multilayers on different surfaces was successfully achieved.[70,71] Furthermore, the investigation of the local magnetic properties of the 6 nm superparamagnetic CsNiCr particles was achieved on patterned surfaces using combined top-down and bottom-up approaches.[107] Our expertise on the organization of the superparamagnetic nanoparticles on surfaces will be applied on the photomagnetic, spin-crossover, and luminescent nanostructures. One of the challenges is to investigate the magnetic behavior of a single object and eventually to tune the property of one nanoparticle by an external stimulus. Spin-crossover nanoparticles are very promising because application for data storage and signal treatment may be accessible at room temperature.

The manipulation of the nanoparticles in solution for the purpose of their organization or for their integration into devices requires a fine control of their surface chemistry. Encouraging results were obtained because of the stabilization of surfactant-free charged particles, which enables a subsequent coating of the particles by an adequate component (see the section on Bimetallic Superparamagnetic CNPs), allowing the introduction of new functions for biocompatibility, biosensing, or electroactivity, for instance.

We have shown that the concept of CNPs is not confined to bimetallic cyanide-bridged systems but can be extended to any coordination network, allowing introduction of a property other than magnetism and opening the possibility of designing multiproperty nanostructured particles. A promising family in this respect is the one based on bridging oxalate, where the bidentate nature of the oxalate ligand allows the appearance of chirality. The 2D anionic nature of the oxalate-bridged networks allowed the introduction of different components in the interlayer space and thus the design of multifunctional systems.[6,9,11,16,20,108] The nanostructuration of such networks will clearly lead to multifunctionality at the nanoscale.

Finally, we consider that lanthanide containing CNPs are very promising for biological applications as labels and contrast agents. Gd-based cyanide-bridged and terephtalate-bridged CNPs were synthesized in our group using the same procedure as for the Tb and Eu-based luminescent particles. Recent examples have been reported providing evidence of the large relaxivities enhancements.[74,78] However, isolation of sub-20nm Gd-based biocompatible CNPs stable in physiological conditions is still an important goal to reach for MRI applications.

Acknowledgment. We thank the CNRS (Centre National de la Recherche Scientifique), the French programme Nanoscience (ACI SupNanoMol NR0142), the Région Ile-de-France (Nanoscience Competence Center of the Région Ile-de France, C'Nano IdF), and the European community (Contracts MRTN-CT-2003-504880 and NMP3-CT-2005-515767 NoE "MAGMANET") for financial support.

IC8012574

(107) Ghirri, A.; Candini, A.; Evangelisti, M.; Gazzadi, G. C.; Affronte, M.; Volatron, F.; Fleury, B.; Catala, L.; David, C.; Mallah, T. *Small* **2008**, DOI: 10.1002/smll.

(108) Train, C.; Gheorghe, R.; Krstic, V.; Chamoreau, L.-M.; Ovanesyan, N. S.; Rikken, G. L. J. A.; Gruselle, M.; Verdaguer, M. *Nature Materials* **2008**, *7*, 729–734.